

The Chiral Non-Centrosymmetric Superconductors TaRh₂B₂ and NbRh₂B₂

Elizabeth M. Carnicom^{1*}, Weiwei Xie², Tomasz Klimczuk³, Jingjing Lin⁴,
Karolina Górnicka³, Zuzanna Sobczak³, Nai Phuan Ong⁴, and Robert J. Cava^{1*}

¹*Department of Chemistry, Princeton University, Princeton, New Jersey 08544, USA*

²*Department of Chemistry, Louisiana State University, Baton Rouge, Louisiana 70803, USA*

³*Department of Physics, Gdansk University of Technology, Gdansk 80-233, Poland and*

⁴*Department of Physics, Princeton University, Princeton, New Jersey 08544, USA*

The symmetry of a material's crystal structure has a significant effect on the energy states of its electrons. Inversion symmetry, for example, results in energetically degenerate electron energy bands for electrons with wave vectors \mathbf{k} and $-\mathbf{k}$, but, when spatial inversion symmetry is absent, this equivalence is no longer possible. In a non-centrosymmetric superconductor, such inequivalence has an important effect: the standard superconducting state, where electrons with opposite momenta form pairs on the Fermi surface, is not possible. A handful of such materials is known; they display different degrees of influence of this lack of inversion symmetry on their superconducting properties. The effect of crystal structure chirality on the properties and applications of superconductors, on the other hand, is little discussed. Here we report the new isostructural non-centrosymmetric superconductors TaRh₂B₂ and NbRh₂B₂, which have a previously unreported crystal structure type. Not only do these materials lack inversion symmetry, but their crystal structure is also chiral; in other words, they can exist in right-handed or left-handed forms. Unlike most superconductors, their upper critical magnetic fields extrapolated to 0 K exceed the Pauli limit, which is often taken as the first indication that a superconducting material is anomalous. We propose that these materials represent a new kind of platform on which the effects of handedness on superconductors and their devices can be tested.

I. INTRODUCTION

The discovery of superconductivity in CePt₃Si^{1,2} has sparked interest in superconductors with non-centrosymmetric crystal structures³ and their anomalous character.^{4,5} By far, most superconductors reported to date possess inversion symmetry, believed to be a favorable trait in a superconducting material. When a superconductor has an inversion center, it can be classified as having either spin singlet or spin triplet pairing since the resulting spin degeneracy is protected by the inversion.^{6,7} However, for non-centrosymmetric crystal structures, conventional Cooper pairs can no longer form since a state on the Fermi surface with momentum \mathbf{k} does not have a degenerate pair at $-\mathbf{k}$.⁸ When inversion symmetry is absent, anti-symmetric spin-orbit coupling (ASOC) breaks the degeneracy, and states of mixed parity become possible, which can result in complicated spin structures.^{9,10} Such an admixture of spin states results in quasiparticle band structures that are topologically non-trivial, which in turn results in a material with protected zero-energy states at the surface or edges, similar to topological insulators.^{11,12}

The violation of parity conservation can lead to various other exotic behaviors, like magnetoelectric coupling¹³ or anomalous upper critical field ($\mu_0 H_{c2}$) values.³ Some non-centrosymmetric superconductors have been shown to have upper critical fields that exceed the Pauli limit ($\mu_0 H^{\text{Pauli}} = 1.85 T_c$)^{14,15}, a limit that is based on the maximum magnetic field that will not break apart a singlet Cooper pair at low temperatures.¹⁶ Often the interplay between breaking inversion symmetry and superconductivity becomes difficult to unravel when other fac-

tors like heavy fermion behavior¹⁷, as seen in CePt₃Si¹, or magnetism⁵ are present. Studying superconductivity in transition-metal containing non-centrosymmetric compounds such as Mg₁₀Ir₁₉B₁₆,^{18,19} Nb_{0.18}Re_{0.82},²⁰ T₂Ga₉ ($T = \text{Rh, Ir}$),²¹ Li₂T₃B ($T = \text{Pd, Pt}$),^{22,23} or other non-magnetic analogs,^{24,25} such as LaPt₃Si²⁶, is important because factors like the strong correlation of f -electrons and magnetic interactions are absent. Although Mg₁₀Ir₁₉B₁₆,^{18,19} CePt₃Si,^{1,2} and Nb_{0.18}Re_{0.82}²⁰ are non-centrosymmetric, their crystal structures are non-chiral, in other words they are non-enantiomorphic. Li₂T₃B ($T = \text{Pd, Pt}$)^{22,23} and Mo₃Al₂C²⁷ are both non-centrosymmetric and have chiral crystal structures, but the potential effects of their chirality on superconductivity was not noted. (Chiral crystal structures must also be non-centrosymmetric, but non-centrosymmetric crystal structures are not necessarily chiral.) Interestingly, Sr₂RuO₄^{28,29} and UPt₃³⁰, which are centrosymmetric and therefore achiral, are, nonetheless, two of the main candidates believed to display chiral superconductivity.³¹ Li₂Pt₃B has also been proposed^{22,32} as a candidate for chiral superconductivity. In order for a superconductor to be chiral, the phase of the superconducting gap function, $\Delta(\mathbf{k})$, must wind in either a counter-clockwise or a clockwise direction as \mathbf{k} moves along the Fermi surface.³¹

In this study, we report our discovery and investigation of the symmetrically chiral, non-centrosymmetric superconductors TaRh₂B₂ and NbRh₂B₂; reporting their characterization through single-crystal X-ray diffraction, temperature-dependent electrical resistivity, magnetic susceptibility, and specific-heat measurements. They are isostructural, both forming in the same chiral non-centrosymmetric space group $P 3_1$ (No. 144). We show

that some of their properties are consistent with normal conventional superconducting behavior, but we also find that both TaRh_2B_2 and NbRh_2B_2 display anomalous upper critical fields ($H_{c2}(0)$) values that exceed the Pauli limit. We therefore propose that these chiral, non-centrosymmetric materials may display exotic pairing symmetries in the superconducting state.

II. EXPERIMENTAL METHODS

Experimental Design The starting materials for the synthesis of TaRh_2B_2 and NbRh_2B_2 bulk materials were elemental tantalum (>99.9%, 100 mesh, Alfa), niobium (>99.9%, 200 mesh, Aldrich), rhodium (>99.9%, 325 mesh, Alfa), and boron (submicron particles, Callery Chem.). Powders of the starting materials Ta/Nb, Rh, and B were weighed out in a 1:1.9:2.1 ratio, ground using a mortar and pestle, and pressed into a pellet. The samples were then wrapped in Ta foil, placed in an alumina crucible, and heated in a high vacuum furnace to 1200 °C for 6 hr. Variation from the above loading compositions or heating temperature led to the presence of secondary phases in larger amounts. Attempts to arc-melt TaRh_2B_2 followed by annealing at 1100 °C for 1 week in an evacuated silica tube did not result in a single-phase sample. Samples of TaRh_2B_2 and NbRh_2B_2 are stable in air and do not decompose over time.

Crystal Structure Characterization The purity of the samples studied was checked using room temperature powder X-ray diffraction (pXRD) using a Bruker D8 Advance Eco Cu K_α radiation ($\lambda = 1.5406 \text{ \AA}$) diffractometer with a LynxEye-XE detector. Single crystals from an arc-melted and annealed sample of TaRh_2B_2 were mounted on the tips of Kapton loops. A Bruker Apex II X-ray diffractometer with Mo $K_{\alpha 1}$ radiation ($\lambda = 0.71073 \text{ \AA}$) was used to collect room temperature intensity data. The data were collected over a full sphere of reciprocal space with 0.5° scans in ω , 10s per frame of exposure time, and a 2θ range from 4° to 75° . The SMART software was used for acquiring all data and the SAINT program was used to both extract intensities and to correct for polarization and Lorentz effects. XPREP was used to perform numerical absorption corrections.³³ Twinning of the unit cell was tested. The crystal structure of TaRh_2B_2 was solved using direct methods and refined by full-matrix least-squares on F^2 with the SHELXTL package.³⁴ A total of 25 space groups were tested according to the observed Laue symmetry and the space group was determined to be $P 3_1$. To the best of our knowledge, TaRh_2B_2 has a unique structure type. The crystal structure images were created in the program VESTA.³⁵ Since boron is such a light element, and therefore difficult to quantify using X-ray diffraction, the B content determined in the refinement was tested further through synthesis of materials of different boron contents. Such syntheses resulted in significant amounts of impurity phases. Finally, the surfaces of Ta-Rh-B samples were analyzed for their Ta and

Rh content using an FEI Quanta 250FEG scanning electron microscope equipped with an Apollo-X SDD energy-dispersive spectrometer (EDS). EDAX TEAMTM software was used to process the EDS data by using standardless quantitative analysis. The EDS data confirmed a Ta:Rh ratio of 1:2, consistent with the results from the single crystal refinement. The FullProf Suite program was used to perform LeBail refinements on bulk samples of both TaRh_2B_2 and NbRh_2B_2 using Thompson-Cox-Hastings pseudo-Voigt peak shapes. Lattice parameters determined from single crystal data were consistent with those determined from the LeBail fit for TaRh_2B_2 . The same structure with slightly different cell parameters was also found to index the diffraction pattern for NbRh_2B_2 .

Superconducting Property Measurements A Quantum Design Physical Property Measurement System (PPMS) Dynacool was used to measure the temperature and field-dependent magnetization and temperature-dependent electrical resistivity of TaRh_2B_2 and NbRh_2B_2 using a vibrating sample magnetometer (VSM) and resistivity option. Both zero-field cooled (ZFC) and field-cooled (FC) magnetic susceptibility measurements were taken from 1.7 K - 10 K for the Ta-variant and from 1.7 K - 12 K for the Nb-variant with a 10 Oe applied magnetic field. The field-dependent magnetization was measured at various temperatures for both TaRh_2B_2 and NbRh_2B_2 for fields in the range 0 - 150 Oe for the Ta-variant and 0 - 350 Oe for the Nb-variant. The temperature-dependent electrical resistivity measurements were carried out using a standard four-probe method from 300 K - 1.7 K with an applied current of 2 mA and zero applied magnetic field. The resistivity was then measured in the low temperature region from 1.7 K - 7 K for the Ta-variant and 1.7 K - 9 K for the Nb-variant with applied magnetic fields varying from 0 T to 9 T in 0.5 T increments. A 14 T Quantum Design PPMS was used to measure the high field temperature dependent resistivity of both NbRh_2B_2 and TaRh_2B_2 with a 2 mA applied current in 0.5 T increments. Specific heat data for both TaRh_2B_2 and NbRh_2B_2 were collected on a Quantum Design PPMS Evercool II with applied magnetic fields of 0 T and 9 T.

Electronic Structure Calculations The band structures (BS) and density of states (DOS) of TaRh_2B_2 and NbRh_2B_2 were calculated using Wien2K with LDA-type pseudopotentials. The structural lattice parameters obtained from single crystal diffraction experiments for TaRh_2B_2 were used for the calculation. Spin-orbit coupling was included for all atoms. Reciprocal space integrations were completed over an $8 \times 8 \times 4$ Monkhorst-Pack k -points mesh. The convergence criterion for a self-consistent calculation was taken as $1.0 \times 10^{-4} \text{ eV}$.

III. RESULTS AND DISCUSSION

Crystal Structure

Single crystal diffraction was used to determine the

TABLE I. Single crystal crystallographic data for TaRh₂B₂.

Chemical Formula	TaRh ₂ B ₂
Temperature(K)	293(2)K
F.W. (g/mol);	408.39
Space group; <i>Z</i>	<i>P</i> 3 ₁ (No. 144);3
<i>a</i> (Å)	4.6980(7)
<i>c</i> (Å)	8.770(2)
<i>V</i> (Å ³)	167.63(6)
<i>hkl</i> ranges	-7 ≤ <i>h</i> ≤ 7 -13 ≤ <i>l</i> ≤ 13
Absorption Correction	Numerical
Extinction Coefficient	0.0030(6)
θ range (deg.)	5.011–33.159
No. reflections; <i>R</i> _{int}	870; 0.0466
No. independent reflections	760
No. parameters	48
<i>R</i> ₁ ; <i>wR</i> ₂ (<i>I</i> >2 σ (<i>I</i>))	0.0331; 0.0587
<i>R</i> ₁ ; <i>wR</i> ₂ (all <i>I</i>)	0.0430; 0.0626
Goodness of fit	1.146
Diffraction peak and hole (e ⁻ /Å ³)	5.946; -5.241

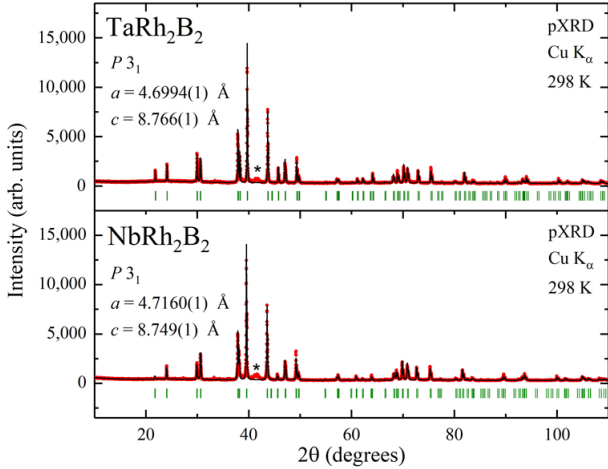


FIG. 1. Room temperature powder X-ray diffraction pattern showing a LeBail fit for the new superconducting phases TaRh₂B₂ (top) and NbRh₂B₂ (bottom). The experimentally observed data are shown with red circles, the calculated pattern is shown with a black line, and the green vertical marks indicate the expected Bragg reflections for space group *P* 3₁ (No. 144). Impurity peaks are marked with asterisks.

crystal structure of the new superconductor TaRh₂B₂, which crystallizes in the chiral, non-centrosymmetric space group *P* 3₁ (No. 144), where *a* = 4.6980(7) Å and *c* = 8.770(2) Å. The crystal structure is reported here for the first time. The space group and lattice parameters from the single crystal refinement were used as a starting point for the LeBail fits of the room temperature pXRD patterns in Fig. 1 for TaRh₂B₂ (top) and isostructural NbRh₂B₂ (bottom). Only standard solid-state synthe-

TABLE II. Atomic coordinates and equivalent isotropic displacement parameters of TaRh₂B₂ at 293(2) K. *U*_{eq} is defined as one-third of the trace of the orthogonalized *U*_{ij} tensor (Å²).

Atom	Wyck.	Occ.	<i>x</i>	<i>y</i>	<i>z</i>	<i>U</i> _{eq}
Ta	3 <i>a</i>	1	0.8481(2)	0.8481(2)	0.3131(2)	0.0041(2)
Rh1	3 <i>a</i>	1	0.6638(4)	0.4824(4)	0.0447(3)	0.0058(2)
Rh2	3 <i>a</i>	1	0.3324(4)	0.8190(4)	0.1072(2)	0.0058(3)
B1	3 <i>a</i>	1	0.627(7)	0.550(8)	0.549(3)	0.012(5)
B2	3 <i>a</i>	1	0.288(9)	0.347(8)	0.215(3)	0.028(5)

sis methods resulted in making the nearly single-phase bulk samples whose powder patterns are shown in Fig. 1. The 3₁ screw axis in the structure, which results in its chirality, can be seen in Fig. 2 (left) when the structure is viewed along the *a*-direction. In addition, viewing the structure along the *c*-direction (Fig. 2, right) emphasizes the non-centrosymmetric nature of the material. A summary of the single crystal structure refinement for TaRh₂B₂ is given in Table I. The atomic coordinates from the crystal structure refinement are shown in Table II. The new superconducting materials TaRh₂B₂ and isostructural NbRh₂B₂ have crystal structures that are both chiral and non-centrosymmetric.

Magnetic Susceptibility To characterize the superconductors TaRh₂B₂ and NbRh₂B₂, the field-dependent volume magnetization (*M*_V) was measured at 1.7 K (in the superconducting state) for both TaRh₂B₂ (Fig. 3a, inset) and NbRh₂B₂ (Fig. 3b, inset) and fitted to a line in the low field region (*M*_{fit} = *bH* + *a*). The equation $-b = \frac{1}{4\pi(1-N)}$ was used to estimate the value of the demagnetization factor, *N* (which is based on the sample shape and orientation with respect to the ap-

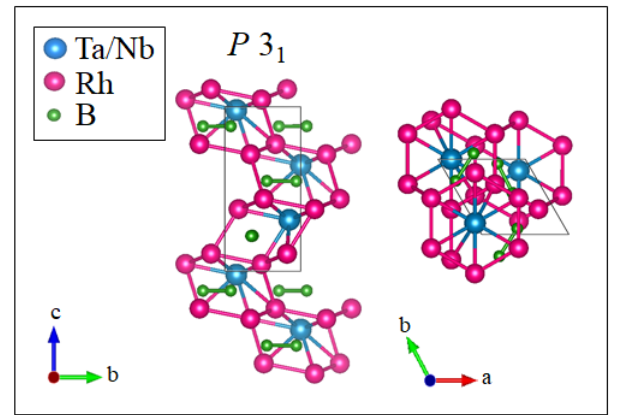


FIG. 2. The crystal structure of chiral and non-centrosymmetric TaRh₂B₂ and isostructural NbRh₂B₂ viewed along the *a*-direction, emphasizing the 3₁ screw axis (left) and along the *c*-direction (right), emphasizing the lack of inversion symmetry. Tantalum/niobium is shown in blue, rhodium is shown in pink, and boron is shown in green.

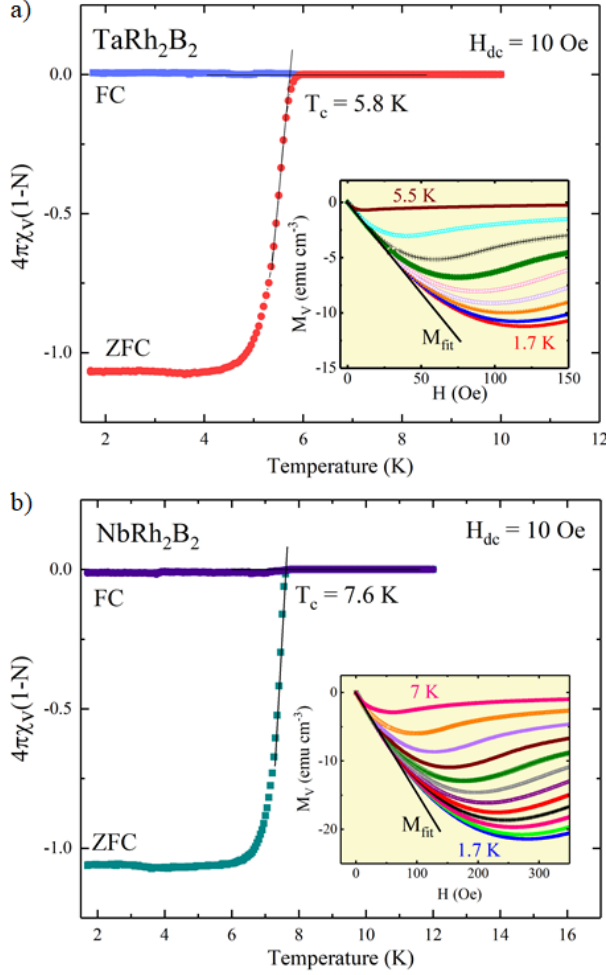


FIG. 3. Zero-field cooled and field cooled temperature-dependent magnetic susceptibility $\chi_V(T)$ for a) TaRh₂B₂ and b) NbRh₂B₂ measured in an applied magnetic field of 10 Oe. Inset: Field-dependent volume magnetization (M_V) measured at various temperatures below T_c . The fit lines M_{fit} were used to estimate the demagnetization factor, N , for both materials. These values were used to correct the magnetic susceptibility data in the main panels.

plied magnetic field), using the slope of the fitted line, b . Further characterization was carried out through both zero-field cooled and field-cooled temperature-dependent magnetic susceptibility measurements with a 10 Oe applied field. The measurement was taken from 1.7 K - 10 K for TaRh₂B₂ (Fig.3a, main panel) showing a superconducting critical temperature of 5.8 K. The T_c was determined as the intersection between the normal state of the magnetic susceptibility extrapolated to lower temperature with the line corresponding to the steepest slope of the diamagnetic signal (indicated by black solid lines).³⁶ ZFC and FC measurements were also performed on the Nb-variant (Fig.3b, main panel) from 1.7 K - 12 K, showing a $T_c = 7.6$ K. Both the ZFC and FC measurements were corrected for $N = 0.504$ for the Ta-variant and N

$= 0.448$ for the Nb-variant. The resulting diamagnetic signal is only slightly less than the ideal value of $4\pi\chi_V(1-N) = -1$ for both TaRh₂B₂ and NbRh₂B₂. The observed critical temperatures in the susceptibility measurements are consistent with both the specific heat and resistivity measurements (discussed next) for each superconducting material. There is a very weak superconducting signal observed for the field-cooled measurement for each material, as expected due to the polycrystalline nature of both samples.

Magnetization The new superconductors TaRh₂B₂ and NbRh₂B₂ were further studied with field-dependent magnetization (M_V) measurements at different temperatures below the critical temperature as seen in Fig.3a (inset) for the Ta-variant and Fig.3b (inset) for the Nb-variant. The low-field linear fits to the magnetization data (M_{fit}), discussed previously, were used to construct the M_V - M_{fit} plot in Fig.4a (inset) for TaRh₂B₂ and NbRh₂B₂ (Fig.4b, inset). The field at which the magnetization begins to deviate from a linear response (indi-

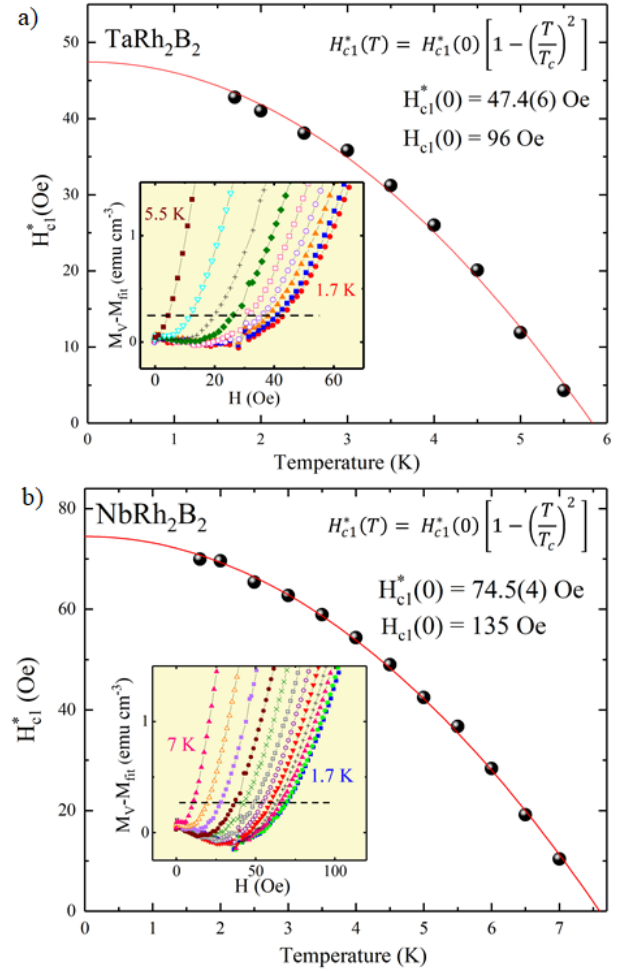


FIG. 4. Estimation of the lower critical field H_{c1}^* vs. temperature for a) TaRh₂B₂ and b) NbRh₂B₂. Inset: Plot of $M_V - M_{fit}$ used to obtain data points to estimate H_{c1}^* .

cated by the black dashed line in each inset) is the uncorrected lower critical field, H_{c1}^* , for that temperature. All the H_{c1}^* values with the corresponding temperatures were plotted in Fig.4a (main panel) for TaRh₂B₂ and in Fig.4b (main panel) for NbRh₂B₂ and fitted to the following equation,

$$H_{c1}^*(T) = H_{c1}^*(0) \left[1 - \left(\frac{T}{T_c} \right) \right]^2, \quad (1)$$

where $H_{c1}^*(0)$ is the lower critical field at 0 K and T_c is the superconducting critical temperature. $H_{c1}^*(0)$ was calculated to be 47.4(6) Oe for TaRh₂B₂ and 74.5(4) Oe for NbRh₂B₂. After correcting for the demagnetization factor for each sample, $H_{c1}(0)$ was calculated to be 96 Oe for the Ta-variant and 135 Oe for the Nb-variant.

Specific Heat and Observed Superconducting Parameters The temperature-dependence of C_p/T is plotted for both TaRh₂B₂ and NbRh₂B₂ in Fig.5a (main panel) under zero applied magnetic field measured from 2 K - 9 K, showing a large anomaly in the specific heat for each superconducting material. Using equal-entropy constructions of the idealized specific heat capacity jump (grey shading), the T_c was determined to be 5.8 K for the Ta-variant and 7.6 K for the Nb-variant, consistent with the magnetic susceptibility and resistivity data.

At low temperature, the specific heat data can be described by the equation

$$\frac{C_p}{T} = \gamma + \beta T^2, \quad (2)$$

where γT is the electronic contribution and βT^3 is the phonon contribution to the specific heat. This linear relationship can be seen in the C_p/T vs T^2 plot in the inset of Fig.5a for TaRh₂B₂ and NbRh₂B₂. By fitting our data to the above equation (using data from the 9 T measurement taken in the normal state), the Sommerfeld parameter γ was calculated to be 5.8(1) mJ mol⁻¹K⁻² for the Ta-analog and 8.8(2) mJ mol⁻¹K⁻² for the Nb-analog. Based on the slope of each fitted line, β was calculated to be 0.178(5) mJ mol⁻¹K⁻⁴ for TaRh₂B₂ and $\beta = 0.203(3)$ mJ mol⁻¹K⁻⁴ for NbRh₂B₂. The Debye model was then used with the β value in the equation

$$\Theta_D = \left(\frac{12\pi^4}{5\beta} nR \right)^{\frac{1}{3}} \quad (3)$$

to calculate the Debye temperature Θ_D , where $n = 5$ (TaRh₂B₂ or NbRh₂B₂) and R is the gas constant 8.314 J mol⁻¹ K⁻¹. The Debye temperatures were calculated to be $\Theta_D = 379$ K and $\Theta_D = 362$ K for the Ta- and Nb-variant, respectively. With Θ_D and T_c , the electron-phonon coupling constant, λ_{ep} , can then be calculated using the inverted McMillan³⁷ equation,

$$\lambda_{ep} = \frac{1.04 + \mu^* \ln \left(\frac{\Theta_D}{1.45T_c} \right)}{(1 - 0.62\mu^*) \ln \left(\frac{\Theta_D}{1.45T_c} \right) - 1.04}, \quad (4)$$

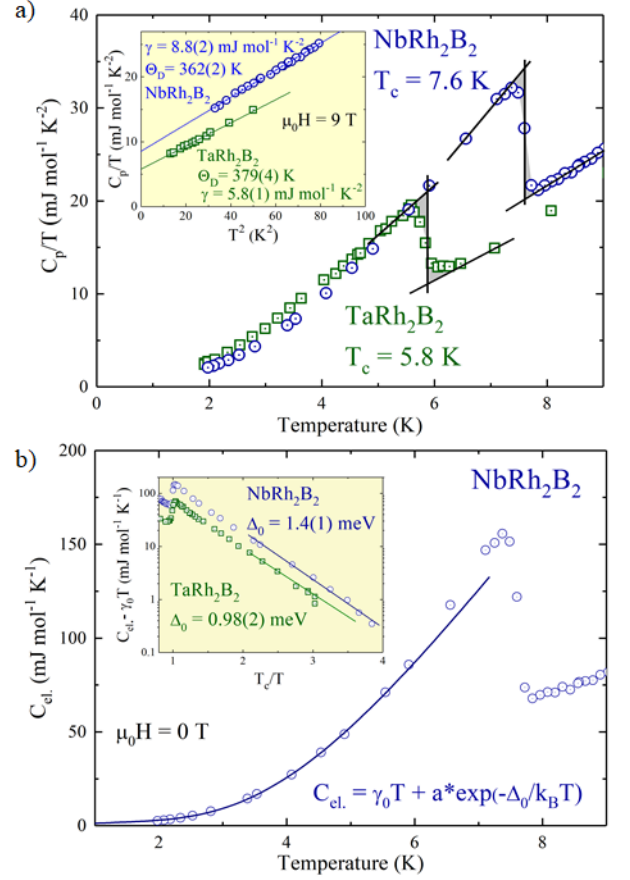


FIG. 5. a) C_p/T vs. T plotted from 0 K - 9 K for TaRh₂B₂ (green open squares) and NbRh₂B₂ (blue open circles) measured in zero applied field where the solid black lines outline the equal area construction shown with grey shading. This construction is used for the estimation of T_c and the superconducting jump $\Delta C/T_c$. Inset: C_p/T vs. T^2 measured in a 9 T field (in the normal state) fitted to $C_p/T = \gamma + \beta T^2$. b) Temperature dependent electronic specific heat C_{el} for NbRh₂B₂ below 9 K. The solid curve through the data is a fit by a one-gap BCS model for superconductivity. Inset: $C_{el} - \gamma_0 T$ vs. normalized temperature (T_c/T) for NbRh₂B₂ and TaRh₂B₂.

where $\mu^* = 0.13$ and $T_c = 5.8$ K and 7.6 K, respectively. The superconducting parameter $\lambda_{ep} = 0.62$ and 0.69 for TaRh₂B₂ and NbRh₂B₂, suggesting that both materials are weak-moderate coupling superconductors. Using λ_{ep} , γ , and the Boltzmann constant k_B , the density of electronic states at the Fermi energy $N(E_F)$ can be calculated from the equation

$$N(E_F) = \frac{3\gamma}{\pi^2 k_B^2 (1 + \lambda_{ep})}. \quad (5)$$

$N(E_F)$ was estimated to be 2.46 states eV⁻¹ per formula unit of TaRh₂B₂ and 3.74 states eV⁻¹ per formula unit of NbRh₂B₂, respectively. In addition, the normalized specific heat jump, $\Delta C/\gamma T_c$, was found to be 1.56 and 1.60 for the Ta- and Nb-analogs, both of which are larger

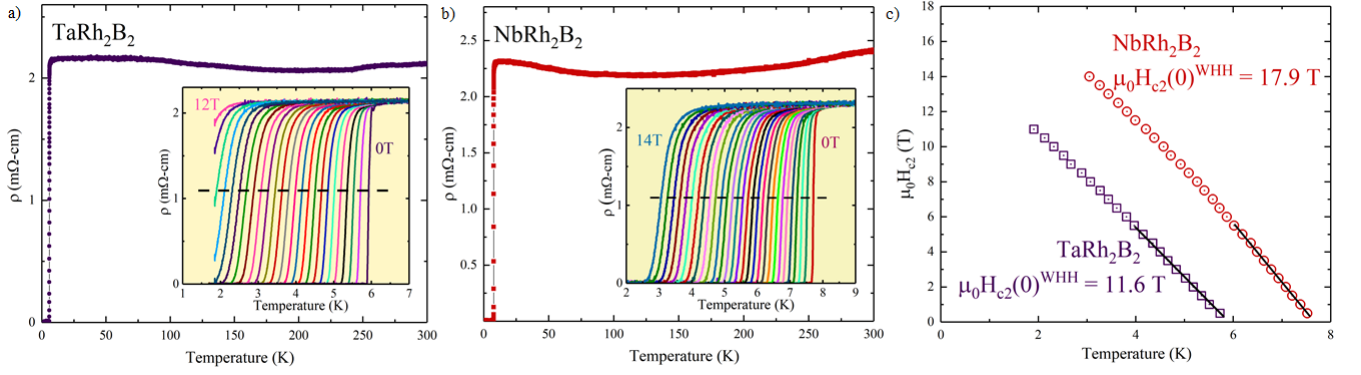


FIG. 6. Temperature-dependent electrical resistivity of a) TaRh₂B₂ and b) NbRh₂B₂ measured from 300 K - 1.7 K with zero applied magnetic field. Inset: Plot of the dependence of the superconducting transition on applied magnetic field measured from a) 1.7 K - 7 K for the Ta-variant in applied fields from 0 T - 12 T and b) from 1.7 K - 9 K for the Nb-variant in applied magnetic fields from 0 T to 14 T in 0.5 T increments. The dashed black line shows 50 % of the superconducting transition. c) The T_c values at different applied fields were used to calculate $\mu_0 H_{c2}(0)$ to be 11.6 T for TaRh₂B₂ and 17.9 T for NbRh₂B₂.

than the expected value of 1.43, which suggests that both materials are moderately-coupled superconductors.

Fig.5b (main panel) shows low temperature (below T_c) electronic specific heat, C_{el} , vs. T for NbRh₂B₂ in zero applied field and fitted to the equation

$$C_{el} = \gamma_0 T + a * e^{-\frac{\Delta_0}{k_B T}}, \quad (6)$$

where k_B is the Boltzmann constant, $\gamma_0 T$ is the electronic contribution to the specific heat coming from the sample impurities, and Δ_0 is the magnitude of the superconducting gap. $C_{el} - \gamma_0 T$ plotted as a function of the normalized T_c/T for both TaRh₂B₂ and NbRh₂B₂ is shown in the inset of Fig.5b. For a weak coupling superconductor,

$$2\Delta_0 = 3.5k_B T. \quad (7)$$

For TaRh₂B₂, the obtained value $\Delta_0 = 0.98$ meV (for which $2\Delta_0 = 1.96$ meV) is larger than the theoretical value of $2\Delta_0 = 1.75$ meV (for $T_c = 5.8$ K). Likewise for NbRh₂B₂, the calculated value of $\Delta_0 = 1.4$ meV ($2\Delta_0 = 2.8$ meV) for $T_c = 7.6$ K is larger than the expected value of $2\Delta_0 = 2.29$ meV, which is consistent with what was proposed previously that TaRh₂B₂ and NbRh₂B₂ are moderately-coupled superconductors.

Resistivity The temperature dependent electrical resistivity measured from 300 K - 1.7 K for TaRh₂B₂ is shown in Fig.6a (main panel) and for NbRh₂B₂ in Fig.6b (main panel). The resistivity drops to zero at 5.8 K for the Ta-variant and at 7.7 K for the Nb-variant. These new materials are both poor metals and the resistivity is essentially temperature independent for the temperature range above T_c . The dependence of T_c , taken as 50 % of the resistivity transition (black dashed line), on the applied magnetic field is shown in the inset of Fig.6a for TaRh₂B₂ and Fig.6b for NbRh₂B₂ where the field is increased from 0 T - 12 T in 0.5 T increments for the Ta-variant and from 0 T - 14 T for the Nb-variant. Even

with a 11 T applied magnetic field, the critical temperature was only suppressed to ~ 1.9 K for the Ta-variant and to ~ 3 K for the Nb-variant in a 14 T applied magnetic field. Fig.6c shows the upper critical fields $\mu_0 H_{c2}$ plotted as a function of the estimated T_c values and fitted to a line close to T_c for TaRh₂B₂ and NbRh₂B₂. The resulting slope ($d\mu_0 H_{c2}/dT$) is -2.9 T/K for TaRh₂B₂ and -3.4 T/K for NbRh₂B₂. The 0 K upper critical field, $\mu_0 H_{c2}(0)$, can then be estimated using the Werthamer-Helfand-Hohenberg (WHH) equation,³⁸

$$\mu_0 H_{c2}(0) = -AT_c \left. \frac{d\mu_0 H_{c2}}{dT} \right|_{T=T_c}, \quad (8)$$

where A is 0.693 for the dirty limit (which will be discussed later). Using $T_c = 5.8$ K for the Ta-analog and $T_c = 7.6$ K for the Nb-analog, the dirty limit $\mu_0 H_{c2}(0)$ values were calculated to be 11.6 T and 17.9 T, respectively. Both of which are high and even exceed the Pauli limit ($\mu_0 H^{\text{Pauli}} = 1.85 * T_c$), where $\mu_0 H^{\text{Pauli}} = 10.7$ T for TaRh₂B₂ and $\mu_0 H^{\text{Pauli}} = 14.1$ T for NbRh₂B₂. Even with a 14 T applied magnetic field, (which is essentially equal to the Pauli limit for NbRh₂B₂) the T_c was only suppressed to 3 K, confirming a $\mu_0 H_{c2}(0)$ value that exceeds the Pauli limit. Likewise, for TaRh₂B₂, the last measurable T_c value was 1.9 K at 11 T, which is already above the Pauli limit for this material. A higher than expected $\mu_0 H_{c2}(0)$ value has also been seen in non-centrosymmetric superconductor CePt₃Si^{1,2}, as discussed previously, which is a good indication that the superconductors reported here are anomalous. The determined $\mu_0 H_{c2}(0)$ and $H_{c1}(0)$ values can be used to calculate several other superconducting parameters. Using the equation

$$H_{c2}(0) = \frac{\Phi_0}{2\pi\xi_{GL}^2}, \quad (9)$$

where Φ_0 is the quantum flux $h/2e$, the Ginzburg-

TABLE III. Observed superconductivity parameters of TaRh₂B₂ and NbRh₂B₂.

Parameter	Units	TaRh ₂ B ₂	NbRh ₂ B ₂
T_c	K	5.8	7.6
$\mu_0 H_{c1}(0)$	mT	9.6	13.5
$\mu_0 H_{c2}(0)$	T	11.6	17.9
$\mu_0 H_c(0)$	mT	169	248
ξ_{GL}	Å	53	43
λ_{GL}	Å	2586	2190
κ_{GL}	-	48	51
γ	mJ mol ⁻¹ K ⁻²	5.8	8.8
$\Delta C/\gamma T_c$	-	1.56	1.60
$\mu_0 H^{\text{Pauli}}$	T	10.7	14.1
λ_{ep}	-	0.62	0.69
$N(E_F)$	states eV ⁻¹ per f.u.	2.46	3.74
Θ_D	K	379	362
Δ_0	meV	0.98	1.4

Landau coherence length ξ_{GL} was calculated to be 53 Å for TaRh₂B₂ and 43 Å for NbRh₂B₂. The dirty limit (discussed previously) was used to determine $\mu_0 H_{c2}(0)$ since the obtained ratio of the coherence length ξ_{GL} and the mean free path (l) was greater than 1. The mean free path was determined using the following equation (derived in Ref.³⁹),

$$l = 2.372 \times 10^{-14} \left(\frac{m^*}{m_e} \right)^2 \frac{V_M^2}{N(E_F)^2 \rho}, \quad (10)$$

where V_M is the molar volume, ρ is the resistivity, and $N(E_F)$ is the density of states at the Fermi level. For TaRh₂B₂, $V_M = 33.6 \text{ cm}^3 \text{ mol}^{-1}$, $\rho = 2 \text{ m}\Omega\text{-cm}$, $N(E_F) = 2.46 \text{ states eV}^{-1} \text{ per f.u.}$, and assuming that $m^*/m_e = 1$, we obtain $l = 22 \text{ Å}$. Similarly, for NbRh₂B₂, $V_M = 39.0 \text{ cm}^3 \text{ mol}^{-1}$, $\rho = 2.2 \text{ m}\Omega\text{-cm}$, and $N(E_F) = 3.74 \text{ states eV}^{-1} \text{ per f.u.}$, which gives $l = 12 \text{ Å}$. The resulting ratios of ξ_{GL}/l are 2.4 and 3.7 for the Ta- and Nb-variant, respectively, showing that both TaRh₂B₂ and NbRh₂B₂ are in the dirty limit.

Using the result of ξ_{GL} with H_{c1} (determined previously), the superconducting penetration depth $\lambda_{GL} = 2586 \text{ Å}$ for the Ta-analog and 2190 Å for the Nb-analog were estimated using the lower critical field equation:

$$H_{c1} = \frac{\Phi_0}{4\pi\lambda_{GL}^2} \ln \frac{\lambda_{GL}}{\xi_{GL}}. \quad (11)$$

The value $\kappa_{GL} = \lambda_{GL}/\xi_{GL}$ was calculated to be $\kappa_{GL} = 48$ for TaRh₂B₂ and $\kappa_{GL} = 51$ for NbRh₂B₂, confirming type-II superconducting behavior in both new materials. Combining the results of H_{c1} , H_{c2} , and κ_{GL} , the thermodynamic critical field can be estimated from the equation,

$$H_{c1}H_{c2} = H_c^2 \ln \kappa_{GL}. \quad (12)$$

This calculation yields $\mu_0 H_c = 169 \text{ mT}$ for the Ta-variant and 248 mT for the Nb variant. Table III gives a summary of all the calculated superconducting parameters for the chiral, non-centrosymmetric superconductors TaRh₂B₂ and NbRh₂B₂.

Electronic Structure

To gain an intrinsic insight into the relationship between the superconductivity observed and the electronic states of TaRh₂B₂ and NbRh₂B₂, we investigated the electronic density of states (DOS) and band structure (BS) for both superconducting materials without and with spin-orbit coupling (SOC) (Fig.7). The total and partial density of states for TaRh₂B₂ and NbRh₂B₂ are illustrated in Fig.7c and Fig.7f. The DOS in the energy below -2.0 eV mainly consists of Ta/Nb and Rh *s*- and *d*-orbitals. The DOS in the energy range from -2.0 eV to +2.0 eV contains mixed Ta/Nb and Rh *s*- and *d*-orbitals in addition to *s*- and *p*- orbitals from B, in particular, around the Fermi level. A sharp peak in the DOS is often taken to be an indication of a nearby structural, electronic, or magnetic instability such as superconductivity. To investigate further, we calculated the band structure both with/without spin-orbit coupling for TaRh₂B₂ (Fig.7a-b) and for NbRh₂B₂ (Fig.7d-e). The broad peak

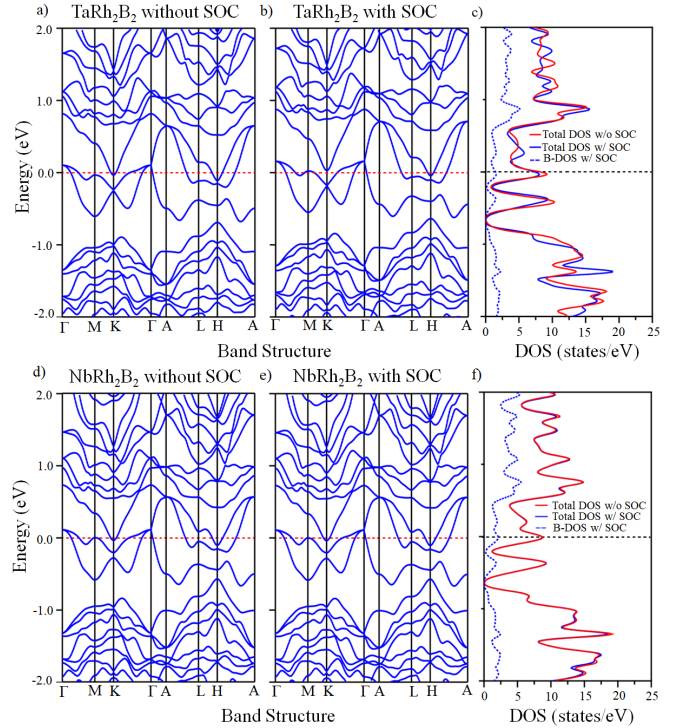


FIG. 7. Calculated band structure for a-b) TaRh₂B₂ and d-e) NbRh₂B₂ both with (middle) and without (left) spin-orbit coupling plotted in the energy range from -2.0 to 2.0 eV. The total density of states (DOS) calculated using the Wien2K with LDA-type pseudopotentials with spin-orbit coupling included (blue line) and without SOC (red line) for c) TaRh₂B₂ and f) NbRh₂B₂.

in the DOS at E_F is due to the presence of saddle points in the electronic structure at the M and L points in the Brillouin zone. Saddle points near E_F are often proposed to be important for yielding superconductivity⁴⁰ and may also be significant in the current materials.

IV. CONCLUSIONS

In summary, we report two new non-centrosymmetric superconductors, TaRh_2B_2 and NbRh_2B_2 , which both have a new crystal structure belonging to the chiral space group $P 3_1$. Temperature-dependent electrical resistivity, magnetic susceptibility, and specific heat data confirmed bulk superconductivity with $T_c = 5.8$ K for the Ta-analog and $T_c = 7.6$ K for the Nb-analog. The derived superconducting parameters show that TaRh_2B_2 and NbRh_2B_2 are basically type-II BCS moderately-coupled superconductors. However, their behavior under applied magnetic fields shows that $\mu_0 H_{c2}(0)$ exceeds the Pauli limit for both superconducting materials, suggesting a possible triplet superconducting state, but further study would be required to confirm this. Future work on these materials to determine the effects of their chiral non-centrosymmetric symmetry on their normal and superconducting properties, and on their use in advanced devices, particularly those with chirality junctions, will be of future interest.

ACKNOWLEDGEMENTS

The materials synthesis was supported by the Department of Energy, Division of Basic Energy Sciences, Grant No. DE-FG02-98ER45706, and the property characterization was supported by the Gordon and Betty Moore Foundation EPiQS initiative, Grant No. GBMF-4412. The work at LSU was supported by the Board of Regents Research Competitiveness Subprogram (RCS) under Contract No. LEQSF(2017-20)-RD-A-08 and LSU-startup funding. The research in Poland was supported by the National Science Centre, Grant No. UMO-2016/22/M/ST5/00435. N. P. O. acknowledges the support of the Gordon and Betty Moore Foundations EPiQS Initiative through Grant No. GBMF4539. J. J. L. was supported by funds from the National Science Foundation, NSF MRSEC Grant No. DMR 1420541.

AUTHOR CORRESPONDENCE

*E.M.C (carnicom@princeton.edu)

*R.J.C. (rcava@exchange.princeton.edu)

-
- ¹ E. Bauer, G. Hilscher, H. Michor, C. Paul, E. W. Scheidt, A. Griбанov, Y. Seropegin, H. Noël, M. Sigrist, and P. Rogl, *Physical Review Letters* **92**, 027003 (2004).
 - ² K. V. Samokhin, E. S. Zijlstra, and S. K. Bose, *Physical Review B* **69**, 094514 (2004).
 - ³ S. Yip, *Annual Review of Condensed Matter Physics* **5**, 15 (2014).
 - ⁴ I. Sugitani, Y. Okuda, H. Shishido, T. Yamada, A. Thamizhavel, E. Yamamoto, T. D. Matsuda, Y. Haga, T. Takeuchi, R. Settai, and Y. Onuki, *Journal of the Physical Society of Japan* **75**, 043703 (2006).
 - ⁵ T. Akazawa, H. Hidaka, T. Fujiwara, T. C. Kobayashi, E. Yamamoto, Y. Haga, R. Settai, and Y. Onuki, *J. Phys.: Condens. Matter* **16**, L29 (2004).
 - ⁶ E. I. Blount, *Physical Review B* **32**, 2935 (1985).
 - ⁷ S. Yip and A. Garg, *Physical Review B* **48**, 3304 (1993).
 - ⁸ R. P. Kaur, D. F. Agterberg, and M. Sigrist, *Physical Review Letters* **94**, 137002 (2005).
 - ⁹ S. Fujimoto, *Journal of the Physical Society of Japan* **76**, 051008 (2007).
 - ¹⁰ T. Grant, A. J. S. Machado, D. J. Kim, and Z. Fisk, *Superconductor Science and Technology* **27**, 035004 (2014).
 - ¹¹ M. Sato and S. Fujimoto, *Physical Review B* **79**, 094504 (2009).
 - ¹² A. P. Schnyder, P. M. R. Brydon, and C. Timm, *Physical Review B* **85**, 024522 (2012).
 - ¹³ V. M. Edelstein, *Physical Review Letters* **75**, 2004 (1995).
 - ¹⁴ V. P. Mineev, *Physical Review B* **71**, 012509 (2005).
 - ¹⁵ N. Kimura, K. Ito, H. Aoki, S. Uji, and T. Terashima, *Physical Review Letters* **98**, 197001 (2007).
 - ¹⁶ A. M. Clogston, *Physical Review Letters* **9**, 266 (1962).
 - ¹⁷ R. Settai, I. Sugitani, Y. Okuda, A. Thamizhavel, M. Nakashima, Y. Onuki, and H. Harima, *Journal of Magnetism and Magnetic Materials* **310**, 844 (2007).
 - ¹⁸ T. Klimczuk, Q. Xu, E. Morosan, J. D. Thompson, H. W. Zandbergen, and R. J. Cava, *Physical Review B* **74**, 220502 (2006).
 - ¹⁹ T. Klimczuk, F. Ronning, V. Sidorov, R. J. Cava, and J. D. Thompson, *Physical Review Letters* **99**, 257004 (2007).
 - ²⁰ A. B. Karki, Y. M. Xiong, N. Haldolaarachchige, S. Stadler, I. Vekhter, P. W. Adams, D. P. Young, W. A. Phelan, and J. Y. Chan, *Physical Review B* **83**, 144525 (2011).
 - ²¹ T. Shibaayama, M. Nohara, H. Aruga Katori, Y. Okamoto, Z. Hiroi, and H. Takagi, *Journal of the Physical Society of Japan* **76**, 073708 (2007).
 - ²² H. Q. Yuan, D. F. Agterberg, N. Hayashi, P. Badica, D. Vandervelde, K. Togano, M. Sigrist, and M. B. Salamon, *Physical Review Letters* **97**, 017006 (2006).
 - ²³ K. Togano, P. Badica, Y. Nakamori, S. Orimo, H. Takeya, and K. Hirata, *Physical Review Letters* **93**, 247004 (2004).
 - ²⁴ E. Bauer, R. T. Khan, H. Michor, E. Royanian, A. Grytsiv, N. Melnychenko-Koblyuk, P. Rogl, D. Reith, R. Podloucky, E. W. Scheidt, W. Wolf, and M. Marsman, *Physical Review B* **80**, 064504 (2009).
 - ²⁵ M. Isobe, H. Yoshida, K. Kimoto, M. Arai, and E. Takayama-Muromachi, *Chemistry of Materials* **26**, 2155 (2014).

- (2014).
- ²⁶ I. Kawasaki, I. Watanabe, H. Amitsuka, K. Kuniyori, H. Tanida, and Y. Onuki, *Journal of the Physical Society of Japan* **82**, 084713 (2013).
 - ²⁷ A. B. Karki, Y. M. Xiong, I. Vekhter, D. Browne, P. W. Adams, D. P. Young, K. R. Thomas, J. Y. Chan, H. Kim, and R. Prozorov, *Physical Review B* **82**, 064512 (2010).
 - ²⁸ Y. Maeno, H. Hashimoto, K. Yoshida, S. Nishizaki, T. Fujita, J. G. Bednorz, and F. Lichtenberg, *Nature* **372**, 532 (1994).
 - ²⁹ Y. Maeno, S. Kittaka, T. Nomura, S. Yonezawa, and K. Ishida, *Journal of the Physical Society of Japan* **81**, 011009 (2012).
 - ³⁰ J. A. Sauls, *Advances in Physics* **43**, 113 (1994).
 - ³¹ C. Kallin and J. Berlinsky, *Rep. Prog. Phys.* **79**, 054502 (2016).
 - ³² M. Nishiyama, Y. Inada, and G. Q. Zheng, *Physical Review Letters* **98**, 047002 (2007).
 - ³³ SHELXTL, “SHELXTL Software Reference Manual, Version 6.10, Bruker Analytical X-Ray System, Inc., Madison, WI,” (2000).
 - ³⁴ G. M. Sheldrick, *Acta. Crystallography* **A64**, 112 (2008).
 - ³⁵ K. Momma and F. Izumi, *Journal of Applied Crystallography* **44**, 1272 (2011).
 - ³⁶ T. Klimczuk and R. J. Cava, *Physical Review B* **70**, 212514 (2004).
 - ³⁷ W. L. McMillan, *Physical Review* **167**, 331 (1968).
 - ³⁸ N. R. Werthamer, E. Helfand, and P. C. Hohenberg, *Physical Review* **147**, 295 (1966).
 - ³⁹ Y. Singh, C. Martin, S. L. Bud’Ko, A. Ellern, R. Prozorov, and D. C. Johnston, *Physical Review B* **82**, 144532 (2010).
 - ⁴⁰ D. M. Newns, H. R. Krishnamurthy, P. C. Pattnaik, C. C. Tsuei, C. C. Chi, and C. L. Kane, *Physica B* **186-188**, 801 (1993).